Airway basal cell-derived exosomes suppress epithelial-mesenchymal transition of lung cells by inhibiting the expression of ANO1

XIAOHUA GU, ZEYU LIU, SHAN SHAN, TAO REN and SHAOYANG WANG

Department of Respiratory Medicine, Shanghai Jiao Tong University Affiliated Sixth People's Hospital, Xuhui, Shanghai 200233, P.R. China

Received August 17, 2023; Accepted February 8, 2024

DOI: 10.3892/etm.2024.12507

Abstract. Disruption of the epithelial-mesenchymal transition (EMT) of activated lung cells is an important strategy to inhibit the progression of idiopathic pulmonary fibrosis (IPF). The present study investigated the role of exosomes derived from airway basal cells on EMT of lung cells and elucidate the underlying mechanism. Exosomes were characterized by nanoparticle tracking analysis, transmission electron microscopy imaging and markers detection. The role of exosome on the EMT of lung epithelial cells and lung fibroblasts induced by TGF-β1 was detected. RNA sequencing screened dysregulated genes in exosome-treated group, followed by the bioinformatical analysis. One of the candidates, anoctamin-1 (ANO1), was selected for further gain-and-loss phenotype assays. A bleomycin-induced pulmonary fibrosis model was used to evaluate the treatment effect of exosomes. Exosomes were round-like and positively expressed CD63 and tumor susceptibility gene 101 protein. Treatment with exosomes inhibited the EMT of lung cells activated by TGF-β1. 4158 dysregulated genes were identified in exosome-treated group under the threshold of |log2 fold-change| value >1 and they were involved in the metabolism of various molecules, as well as motility-related biological processes. A key gene, ANO1, was verified by reverse transcription-quantitative PCR, whose overexpression induced the EMT of lung cells. By contrast, ANO1 knockdown reversed the EMT induced by TGF-β1. *In vivo* assay indicated that exosome treatment ameliorated pulmonary fibrosis and inhibited the upregulation of ANO1 induced by bleomycin. In conclusion, airway basal cell-derived exosomes suppressed the EMT of lung cells via the downregulation of ANO1. These exosomes represent a potential therapeutic option for patients with IPF.

Correspondence to: Dr Shaoyang Wang or Professor Tao Ren, Department of Respiratory Medicine, Shanghai Jiao Tong University Affiliated Sixth People's Hospital, 600 Yishan Road, Xuhui, Shanghai 200233, P.R. China
E-mail: shaoyang_w@tju.edu.cn
E-mail: rentao305@163.com

Key words: idiopathic pulmonary fibrosis, epithelial-mesenchymal transition, exosomes, anoctamin-1

Introduction

Idiopathic pulmonary fibrosis (IPF) is a progressive, irreversible lung disease with a poor prognosis. It usually occurs in the adults and the 5-year survival rate is only ~20-25%, worse than most types of cancer (1,2). The etiology of IPF remains unknown and it is often characterized by the abnormal activation of alveolar epithelial cells and fibroblasts, leading to the continuous accumulation of collagen and extracellular matrix, ultimately causing structural damage to the lung tissues and lung dysfunction (3). Currently, two drugs, nintedanib and pirfenidone, have been approved for the treatment of IPF, which may delay the progression of IPF to some extent (4). However, their effects remain limited and the search for new molecules or therapeutic strategies continues to be a research hot spots and clinical challenge.

Exosomes are a type of extracellular vesicles with a diameter of 30-150 nm that are released by most eukaryotic cells and circulate in the extracellular environment (5). They are able to carry various types of cellular cargo, including nucleic acids, proteins, lipids and metabolites, thereby playing important roles in intercellular communication. A number of studies have indicated that exosomes secreted from pathological lung cells and the microenvironment exacerbate fibrosis by activating epithelial cells or fibroblasts (6,7). However, exosomes released from the normal lung cells, especially the widely concerned mesenchymal stem cells (MSCs), have been found to show promising therapeutic potential (8,9). MSCs belong to the class of pluripotent stem cells, thus have self-renewal capabilities and are able to differentiate into diverse types of cells (10). In recent decades, MSCs have been highlighted for their potential use in cell therapy for various diseases (11). MSC-derived exosomes have gained attention due to their non-oncogenic and immunogenic characteristics (11). For instance, treatment with bone marrow MSC-derived exosomes was found to inhibit the epithelial-mesenchymal transition (EMT) of lung cells induced by silica, as well as alleviate the progression of fibrosis *in vivo* (12). Some clinical assays have

shown that treatment with MSC-derived exosomes is both safe and effective against some pulmonary diseases, including severe COVID-19 (13,14). In addition, exosomes derived from normal lung cells, namely human bronchial epithelial cell, have also been found to attenuate TGF-β-induced myofibroblast differentiation and lung epithelial cell senescence by inhibiting TGF-β-WNT crosstalk (8).

In our previous study, a rare population of basal cells (SOX9 positive) located at airway epithelium rugae was isolated and identified. These stem-like cells, able to be passaged for at least 30 doublings, were found to regenerate human lung epithelium in patients with chronic lung diseases, as well as rescue dysregulated pulmonary function (15). It has been reported that MSC-derived exosomes are partly responsible for MSC-mediated regeneration (16). Therefore, exosomes derived from basal cells may play vital roles in the recovery of lung function. Thus, it was hypothesized that basal cell-derived exosomes could reverse the activation of lung cells.

EMT is an important pathological change in the activation process of IPF and the disruption of EMT-related effectors can inhibit the occurrence and development of IPF (17). In the present study, the role of basal cell-derived exosomes on the EMT of activated lung cells induced by TGF-β1 was investigated. RNA sequencing was used to identify the dysregulated genes in exosome-treated lung cells. Next, the role of one key gene, anoctamin-1 (ANO1), which encodes the protein recognized as a Ca^{2+}-activated chloride channel (18), in the TGF-β1-induced EMT of lung cells was investigated. Finally, bleomycin-induced pulmonary fibrosis model was used to evaluate the treatment effect of exosomes. The present study is the first to the best of the authors' knowledge to highlight the therapeutic potential of airway basal cell-derived exosomes on IPF. The findings are presented in accordance with the MDAR reporting checklist.

Materials and methods

Cells and cell culture. Primary $SOX9^+$ airway basal cells, accounting for ~1% of the basal cells, were isolated from patients with IFP as reported in a previous study (15) and cultured in DMEM/F12 medium (Gibco; Thermo Fisher Scientific, Inc.) supplemented with 10% fetal bovine serum (FBS; Cytiva), 1% amphotericin, antibiotics and a growth factor cocktail, as previously described (19). Human bronchial epithelial cell line BEAS-2B (cat. no. SCSP-5067) and human embryonic fibroblasts MRC-5 (cat. no. GNHu41) were purchased from the Cell Bank of Chinese Academy of Sciences. BEAS-2B and MRC-5 were cultured with DEME medium (Gibco; Thermo Fisher Scientific, Inc.) and MEM medium (Gibco; Thermo Fisher Scientific, Inc.), respectively, both of which were supplemented with 10% FBS and 1% amphotericin. All cells were maintained in an humidified incubator with 5% CO_2 at 37˚C.

Isolation and identification of exosomes. $SOX9^+$ airway basal cells (within 10 passages) were cultured with exosome-free FBS for 48 h. Then, the resulting supernatant was collected and filtered using a 0.45-μm film to remove cell fragments. Next, Qiagen exoEasy Maxi Kit (Qiagen GmbH) was used to extract exosomes, according to the manufacturer's instructions. The number and size distribution of the resulting exosomes was analyzed using NanoSight NS300 (Malvern Instruments, Inc.). Transmission electron microscopy (TEM) was used to observe the morphology of the exosomes. Briefly, a drop of the diluted exosomes were loaded on a cooper mesh and fixed with 2.5% glutaraldehyde for 5 min at room temperature. After an incubated with 1% phosphotungstic acid for 10 min at temperature, the sample was used for TEM imaging. The exosomal positive protein markers [CD63 and tumor susceptibility gene 101 protein (TSG101)] and negative marker (β-Tubulin) were analyzed using western blotting.

Western blotting. BEAS-2B and MRC-5 were treated with 1 ng/ml TGF-β1 for 24 h before culturing with/without exosomes for an additional 24 h. Cells without any treatment were used as the control group. Next, the cells were lysed with RIPA buffer (Beyotime Institute of Biotechnology) and the proteins in the supernatant were quantified using a BCA kit (Beijing Solarbio Science & Technology Co., Ltd.) after the lysates had been centrifuged at 12,000 x g for 5 min at 4˚C. Then, 10 μg of protein was added and separated in 10% SDS-PAGE and the proteins in the gels were transferred onto PVDF membranes. Subsequently, membranes were blocked with 5% fat-free milk for 1 h at room temperature, which were then incubated with primary antibodies at 4˚C overnight, followed by the secondary antibody for 2 h at room temperature. Finally, the signals were enhanced using ECL Plus Western blotting system kit (Beyotime Institute of Biotechnology). The primary antibodies, namely ANO1 (cat. no. 14476; 1:1,000), vimentin (cat. no. 5741; 1:1,000), E-cadherin (cat. no. 3195; 1:1,000), CD63 (cat. no. 52090; 1:1,000), TSG101 (cat. no. 72312; 1:1,000), β-Tubulin (cat. no. 2146; 1:1,000), Fibronectin (FN1; cat. no. 26836; 1:1,000), Collagen I A1 (COL1A1; cat. no. 72026; 1:1,000), GAPDH (cat. no. 5174; 1:1,000) and secondary antibody HRP-labeled IgG (cat. no. 7074; 1:3,000), were obtained from Cell Signaling Technology, Inc. Gray values of the blot bands were analyzed using ImageJ software (version 1.8.0; National Institutes of Health).

RNA sequencing. After treating the cells (BEAS-2B and MRC-5) with 1 ng/ml TGF-β1 for 24 h or further treatment with $5x10^8$ particles/ml exosomes for 24 h at 37˚C, the total RNA of the four samples was extracted using RNeasy mini kit (Qiagen GmbH). Integrity of total RNA was assessed using the Agilent 2100 Bioanalyzer (Agilent Technologies Inc.). Paired-end libraries were synthesized by using the Stranded mRNA-seq Lib Prep Kit (cat. no. RK20301; ABclonal Biotech Co., Ltd.) in accordance with the manufacturer's protocols. Purified libraries were quantified by Qubit 3.0 Fluorometer (Thermo Fisher Scientific, Inc.) and validated by Agilent 2100 bioanalyzer (Agilent Technologies Inc.) to confirm the insert size and calculate the mole concentration. Cluster was generated by cBot (Illumina, Inc.) with the library diluted to 10 pM and then were sequenced on the Illumina NovaSeq 6000 (Illumina, Inc.). cDNA library construction and RNA sequencing were performed by Shanghai Biotechnology Corporation. Nucleotide length and the direction of sequencing were 150 bp and paired-end respectively. The raw data was deposited in the SRA database and accessible at https://www.ncbi.nlm.nih.gov/sra/PRJNA1051029.

Stringtie software (v1.3.3b; The Center for Computational Biology, Johns Hopkins University) was used to count the fragment within each gene and TMM algorithm was used for normalization. Differential expression analysis for mRNA was performed using the edgeR package in R (version 3.4.3; http://www.R-project.org/) (20). Fragments Per Kilobase Million (FPKM) was used to indicate the expression level of gene. Fold-change (FC) was calculated using the ratio of the mean FPKM of TGF-β1 + exosome group to that of TGF-β1 group. The dysregulated genes in TGF-β1 + exosome group were screened using the threshold of |log2(FC)| value >1 (21). The P-value was not taken as the threshold, as the sample number in each group was less than three.

Bioinformatical analyses. Gene Ontology (GO) and Kyoto Encyclopedia of Genes and Genomes (KEGG) pathway analysis were conducted to determine the biological role of the dysregulated genes via the enrich package in R (version 3.4.3; http://www.R-project.org/) (20). Rich factor was calculated using the ratio of dysregulated_gene_in_this_pathway/dysregulated_gene_in_all_pathway to all_gene_in_this_pathway/all_gene_in_all_pathway. The P-value was used to screen the significant GO terms or KEGG pathways and the top 30 terms or pathways were further screened by rich factor to draw the corresponding bubble chart.

Reverse transcription-quantitative (RT-q) PCR. The total RNA of the $5x10^5$ cells was extracted using a RNeasy mini kit (Qiagen GmbH) according to manufacturer's protocols and quantified on a NanoDrop ND-1000 spectrophotometer (NanoDrop Technologies; Thermo Fisher Scientific, Inc.). Next, 500 ng of RNA was transcribed into cDNA using a ReverTra Ace qPCR RT kit (Toyobo Life Science) following manufacturer's instructions. Then, 2 μl of cDNA (n=3) was mixed with 10 μl of Master SYBR Green I mix (Roche Diagnostics), 1 μl of primers and water to obtain a mixture of 20 μl, which was further reacted on an ABI StepOnePlus Real-Time PCR system (Applied Biosystems; Thermo Fisher Scientific, Inc.). The reaction was performed at 95˚C for 5 min, followed by 40 cycles of 95˚C for 10 sec and 60˚C for 60 sec according to manufacturer's protocols. The relative expression levels of mRNA were calculated using the $2^{-\Delta\Delta Cq}$ method (22) and GAPDH was used as the internal control. The sequences of the primers use are listed in Table I.

Cell transfection. The overexpression vector of ANO1 (pcDNA3.1-ANO1) and its short interfering (si)RNA (si-ANO1) were both synthetized by Sangon Biotech Co., Ltd. Next, the overexpression vector (2.5 μg) and si-ANO1 (2 μg) were transfected into $5x10^5$ cells (BEAS-2B and MRC-5) using Lipofectamine® 3000 (Invitrogen; Thermo Fisher Scientific, Inc.) at 37˚C for 48 h, according to the manufacturer's instructions. The control vector and the si-RNA were also transfected into $5x10^5$ cells (BEAS-2B and MRC-5) as negative control (NC) and si-NC, respectively. Subsequently, cells transfected with vectors were screened by G418 for 10 days, followed by qPCR validation. Cells transfected with siRNAs were directly detected by qPCR to confirm the interference efficiency. si-NC: 5'-UUCUCCGAACGUGUCACGUTT-3', si-ANO1: 5'-CGTGTACAAAGGCCAAGTA-3'.

Table I. Primer sequences used for reverse transcription-quantitative PCR.

Gene	Primer sequence (5'-3')
KRT81	Forward: GCATTGGGGCTGTGAATGTCT
	Reverse: ACCCAGGGAGCTGATACCAC
PCDHGA12	Forward: CACCGGGACTACAAAGGGC
	Reverse: ATAGCGTATCTGGGTGCATCC
ANO1	Forward: CTGATGCCGAGTGCAAGTATG
	Reverse: AGGGCCTCTTGTGATGGTACA
CXCL8	Forward:TTTTGCCAAGGAGTGCTAAAGA
	Reverse: AACCCTCTGCACCCAGTTTTC
CXCL5	Forward: AGCTGCGTTGCGTTTGTTTAC
	Reverse: TGGCGAACACTTGCAGATTAC
GAPDH	Forward: GGAGCGAGATCCCTCCAAAAT
	Reverse:GGCTGTTGTCATACTTCTCATGG

Transwell assay. Cells were collected and resuspended in FBS-free medium. Then, 100 μl of cells at a density of $4x10^5$ cells/ml were seeded into the upper chamber and 600 μl of the complete medium was added into the lower chamber. After 24 h of migration, the residual cells on the Inner layer of the membrane were removed and the migrated cells were fixed with methanol for 20 min at room temperature, followed by staining with 0.1% crystal violet for 15 min at room temperature. Finally, the migrated cells were observed and counted under an inverted microscope.

Animals and treatments. Male C57BL/6 mice (6-8 weeks; 18-22 g) were purchased from Shanghai Laboratory Animal Research Center. All mice were maintained in 12-h light/dark cycle and with free access to food and water. The temperature and relative humidity were maintain at 22±2˚C and 50-60%, respectively. The 18 mice were randomly divided into 3 groups (n=6): Control group, model (bleomycin treatment) group and exosome group (bleomycin as well as exosome treatments). Pulmonary fibrosis was induced with a single intratracheal injection of 2 U/kg bleomycin (Nippon Kayaku Co., Ltd.; cat. no. H20090885) in 30 μl saline as reported (23). Mice administered with same volume of saline were served as controls. At 10 days post bleomycin treatment, exosomes ($10x10^9$ particles/kg) were given for ~30 min/day for 7 consecutive days using a nebulizer (Trek S Portable Compressor Nebulizer Aerosol System; PARI GmbH). At 21 days post bleomycin treatment, all mice were anesthetized by intraperitoneal injection of chloral hydrate (350 mg/kg), then sacrificed by cervical dislocation. Lung tissues were collected for protein detection and histological examination. All experimental procedures were approved by the Animal Welfare Ethics Committee of Shanghai Sixth People's Hospital (approval no. 2023-0374).

Histological evaluation. Pulmonary tissue samples were fixed with 4% paraformaldehyde for 48 h at room temperature, followed by dehydration in graded alcohol and embedding in paraffin. Embedded tissue samples were then cut into 5 μm thick sections and stained with hematoxylin and eosin (H&E)

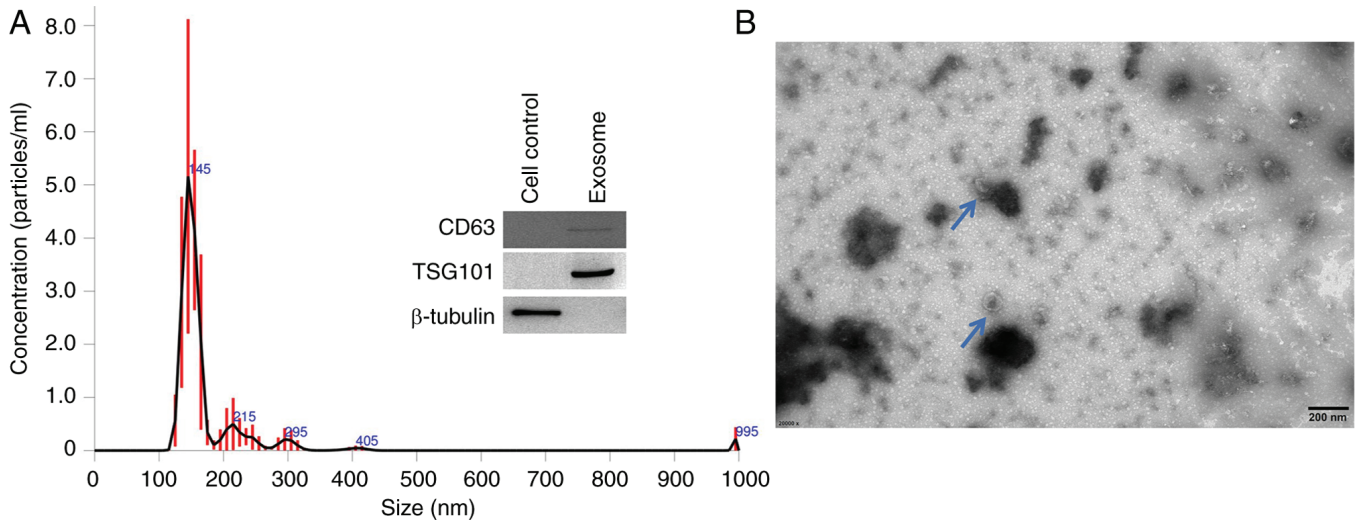

Figure 1. Identification of exosomes derived from airway basal cells. (A) Nanoparticle tracking analysis was performed to detect the particle size distribution of exosomes; (right) western blotting of markers of exosomes. (B) Transmission electron microscopy imaging of the morphology and size of exosomes. Blue arrow indicates the exosomes. Scale bar, 200 nm.

for 5 min or Masson's trichrome reagents for 30 min at room temperature. Images of the histologic sections were captured using light microscopy.

Statistical analysis. Data are presented as the mean ± standard deviation from three independent experiments unless otherwise noted. All statistical analyses were performed using GraphPad Prism 7.0 (Dotmatics). Statistical significance was analyzed by unpaired two-tailed Student's t-test, and one-way ANOVA with Tukey's post hoc test. P<0.05 was considered to indicate a statistically significant difference.

Results

Airway basal cell-derived exosomes suppress the EMT of lung cells induced by TGF-β1. First, the exosomes were extracted from the medium of airway basal cells and the nanoparticle tracking analysis indicated that the majority of the particles had an average diameter of 145 nm, with some showing a larger size (Fig. 1A). The TEM image (Fig. 1B) showed that the obtained particles were round-like and had a size of ~100 nm. Furthermore, exosome makers CD63 and TSG101 were both expressed in these particles, while cellular maker β-Tubulin could not be detected (Fig. 1A, right). These results indicate that the extracellular vesicles were nanoparticles, confirming that they were exosomes.

The resulting exosomes were used to reverse the EMT of activated lung cells. As shown in Fig. 2A, most of the BEAS-2B cells were long shuttle after 1 ng/ml TGF-β1 treatment, then became short shuttle or polygon after further treated with exsomes. Similarly, the morphology of the MRC-5 in TGF-β1 group became more slender compared with the control cells and further treatment of exosomes could reverse this morphological change. Western blot analysis indicated that TGF-β1 stimulation resulted in the significant upregulation of vimentin and the downregulation of E-cadherin in the two types of cells (Fig. 2B and C), reflecting the occurrence of EMT. Notably, the morphological alterations of the two lung cells induced by TGF-β1 were both reversed after further treatment with exosomes. Consistently, the EMT of the two types of cells was also significantly inhibited in the TGF-β1 + exosomes group compared with the TGF-β1 group (Fig. 2B and C). These results suggest that airway basal cell-derived exosomes could relieve the EMT of lung epithelial cell and fibroblasts activated by TGF-β1.

Identification of dysregulated genes in activated lung cells treated with exosomes. To determine the underlying mechanism of the exosomes, the cells in the TGF-β1 and TGF-β1 + exosomes groups were collected and analyzed by RNA sequencing. As shown in Fig. 3A, although the expression profile of the four samples (without any parallels) varied, the fold-change of most genes was consistent in the TGF-β1 + exosomes treated cells compared with the corresponding cells treated with TGF-β1. A total of 4,158 dysregulated genes, including 1,819 upregulated and 2,339 downregulated genes, were screened under the threshold of |log2FC| value >1 (Fig. 3B). The P-value was not taken as the threshold, as the sample number in each group was <3.

As shown in Table II, among the top 20 genes with the highest FC (abs) values, AP005263.1 (unknown gene) had the highest FC (abs) value (1,442), followed by KRT81, PCDHGA12, ANO1 and CXCL8, sharing the FC (abs) values varying from 100-370. The P-value of the 20 genes were also presented and were all <0.05, indicating that the FC (abs) values were consistent in the two independent cells in the TGF-β1 + exosomes group (compared with the cells in TGF-β1 group).

Bioinformatic analysis of dysregulated genes. GO enrichment analysis indicated that the dysregulated genes were enriched in various metabolism processes of quinolinate, glycine and tryptophan (Fig. 4), which were regulated by HAAO, KYNU, ACMSD and KMO (Table SI). Some genes (WNK2, WNK3, ATP1B2 and WNK3) were involved in the biological processes of ion import (Fig. 4, Table SI). The KEGG enrichment results also showed that a number of the pathways were involved in the

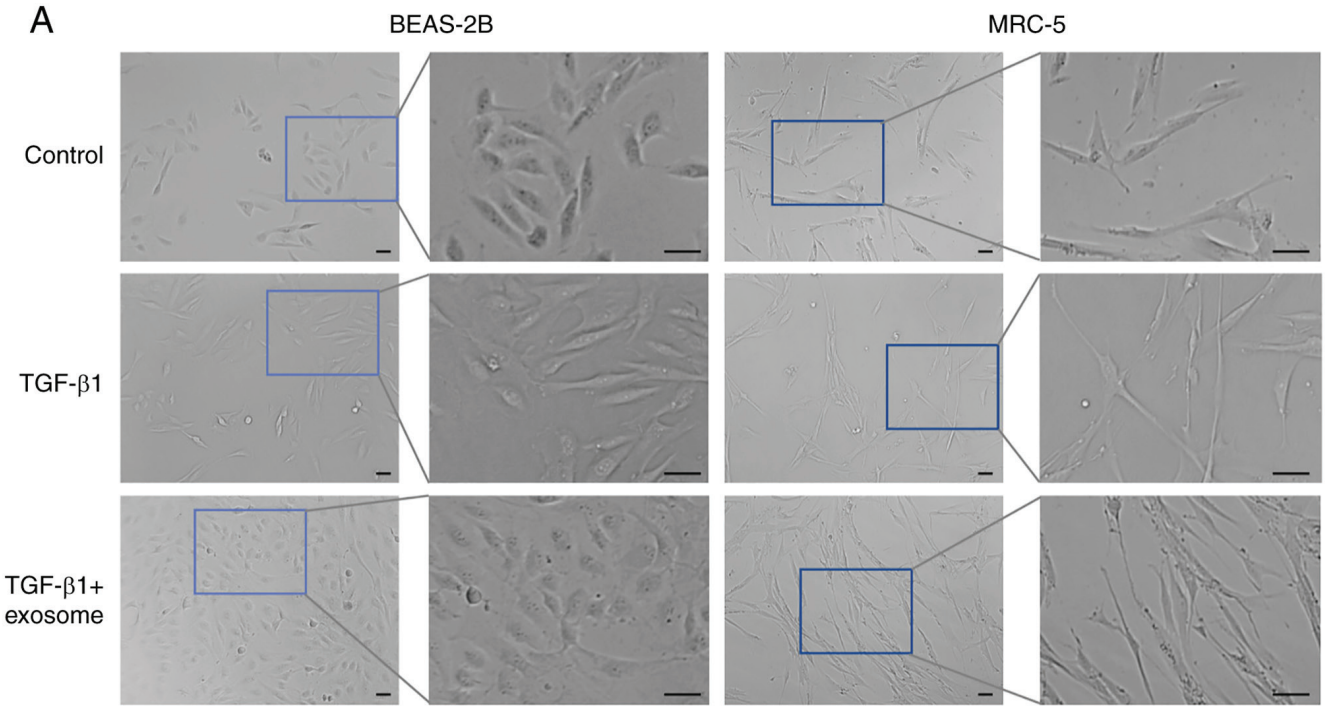

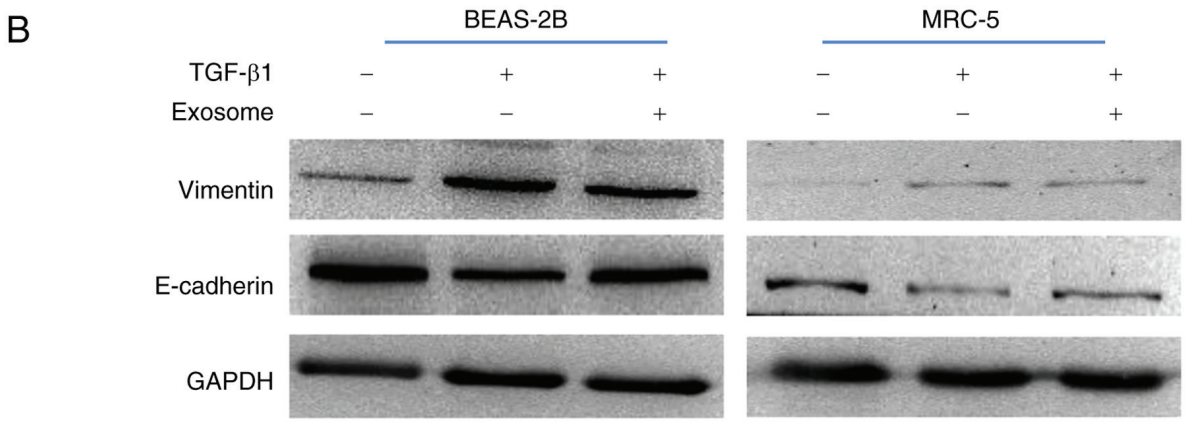

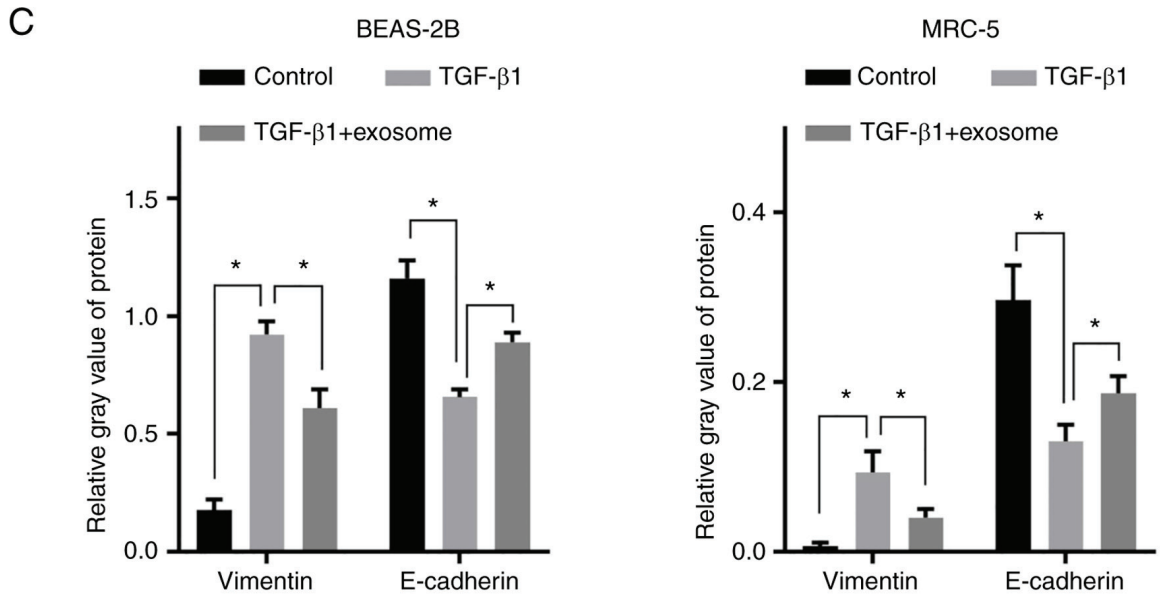

Figure 2. Airway basal cell-derived exosomes suppress the EMT of lung cells induced by TGF-β1. (A) The morphology alterations of lung epithelial cells (BEAS-2B) and lung fibroblasts (MRC-5) were observed after 24 h of exposure to 1 ng/ml TGF-β1 or further treatment with exosomes for 24 h. Scale bar, 50 μm. (B) Western blotting of the protein level of EMT markers (vimentin and E-cadherin) in cells under different treatment conditions (n=3). (C) Quantification analysis result of protein levels. *P<0.05. EMT, epithelial-mesenchymal transition.

Table II. Top 20 dysregulated genes in exosome-treated lung cells.

	Gene id	Gene name	log2FC	log2FC abs	FC abs	P-value
1	ENSG00000265257	*AP005263.1*	10.494	10.494	1442.642	3.54×10^{-9}
2	ENSG00000205426	*KRT81*	8.516	8.516	366.097	4.25×10^{-3}
3	ENSG00000253159	*PCDHGA12*	7.164	7.164	143.379	8.05×10^{-4}
4	ENSG00000131620	*ANO1*	-6.697	6.697	103.749	1.21×10^{-2}
5	ENSG00000169429	*CXCL8*	6.653	6.653	100.627	4.12×10^{-4}
6	ENSG00000163735	*CXCL5*	6.207	6.207	73.892	6.12×10^{-4}
7	ENSG00000157542	*KCNJ6*	-6.135	6.135	70.294	2.53×10^{-2}
8	ENSG00000251537	*AC005324.2*	-5.878	5.878	58.815	1.43×10^{-2}
9	ENSG00000242419	*PCDHGC4*	5.855	5.855	57.871	3.35×10^{-3}
10	ENSG00000286239	*AC093884.1*	-5.840	5.840	57.290	6.71×10^{-3}
11	ENSG00000260108	*AC026464.2*	5.791	5.791	55.373	4.82×10^{-4}
12	ENSG00000118194	*TNNT2*	-5.788	5.788	55.251	5.62×10^{-3}
13	ENSG00000256349	*AP002748.5*	-5.757	5.757	54.069	2.24×10^{-3}
14	ENSG00000149968	*MMP3*	5.688	5.688	51.563	3.43×10^{-3}
15	ENSG00000196611	*MMP1*	5.674	5.674	51.051	3.07×10^{-3}
16	ENSG00000073756	*PTGS2*	5.640	5.640	49.874	3.60×10^{-2}
17	ENSG00000115919	*KYNU*	5.421	5.421	42.852	2.06×10^{-2}
18	ENSG00000105825	*TFPI2*	5.420	5.420	42.825	9.16×10^{-3}
19	ENSG00000123496	*IL13RA2*	5.365	5.365	41.221	4.45×10^{-2}
20	ENSG00000263244	*AC087190.3*	5.326	5.326	40.123	6.11×10^{-3}

FC, fold change; abs, absolute.

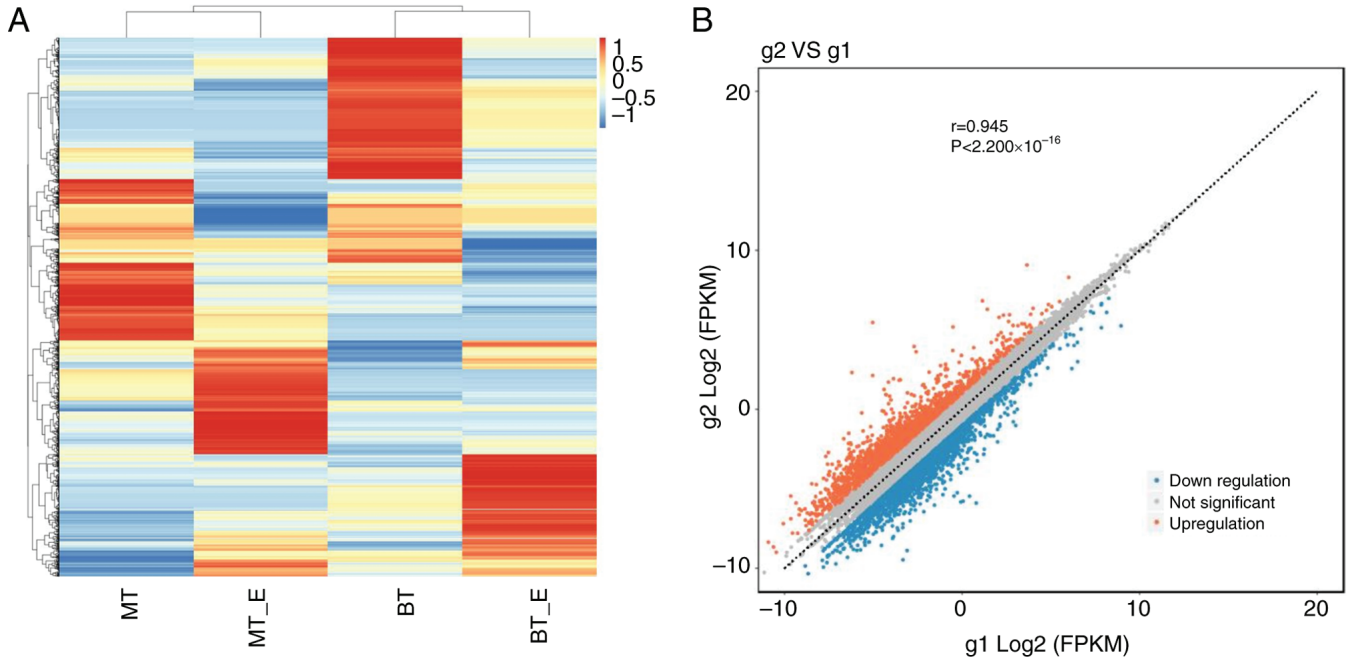

Figure 3. RNA sequencing identification of dysregulated genes. (A) Heatmap of dysregulated genes in four independent cell samples (n=1). (B) Scatter plot of 4158 dysregulated genes under the threshold of |log2 FC| value >1. FC was calculated using the ratio of the mean FPKM of g2 to that of g1. Red or blue dots indicate upregulated or downregulated genes, respectively. FC, fold-change; FPKM, Fragments Per Kilobase Million; BT and MT, BEAS-2B and MRC-5 treated with TGF-β1; BT_E and MT_E, BEAS-2B and MRC-5 treated with TGF-β1 + exosome; g2, TGF-β1 + exosomes group; g1, TGF-β1 group.

metabolism of various amino acids and some other molecules, including thiamine, butanoate and arachidonic acid (Fig. 5). In addition, 51 genes were enriched in cytokine-cytokine receptor interaction and 18 genes were involved in TGF-β signaling pathway, including downregulated NOG, FST, GDF5, BAMBI and BMPR1B (Fig. 5; Table SII).

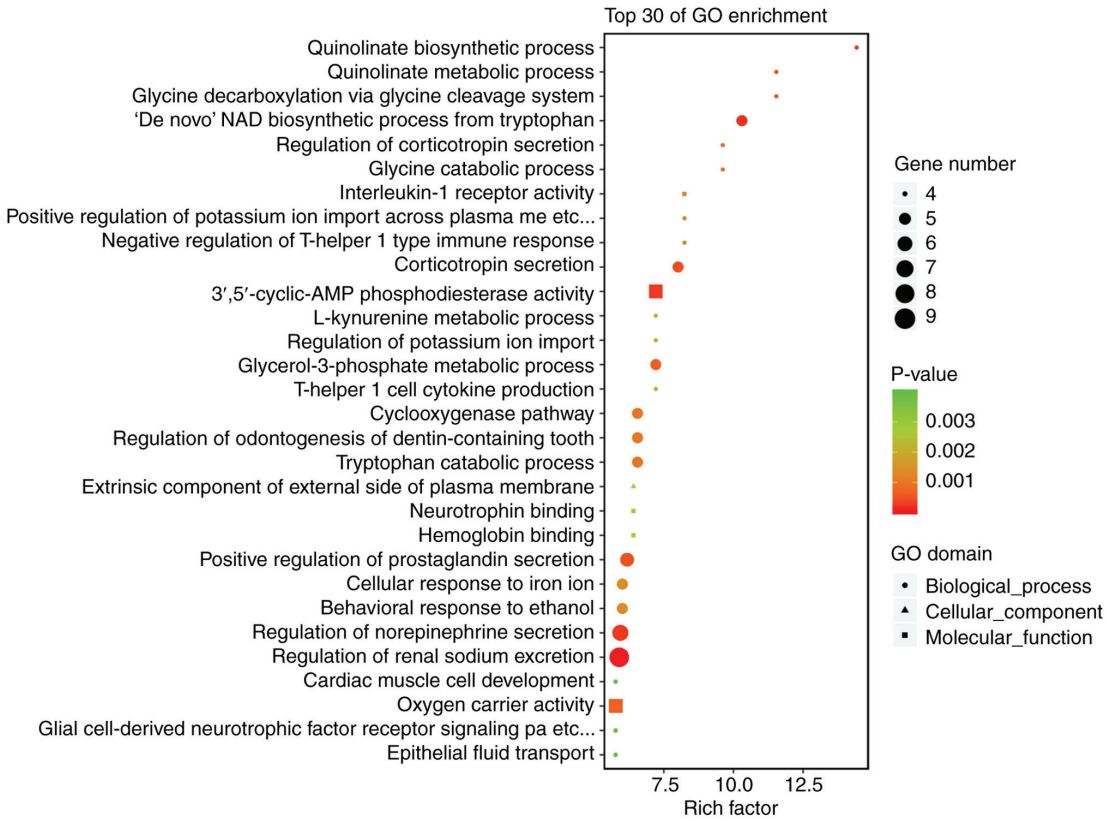

Figure 4. Top 30 GO terms of dysregulated genes. The top 30 GO terms were screened using the rich factor. Circle, triangle and square indicate biological process, cellular component and molecular function, respectively. Their size indicates the gene number and the color indicates the P-value. GO, Gene Ontology.

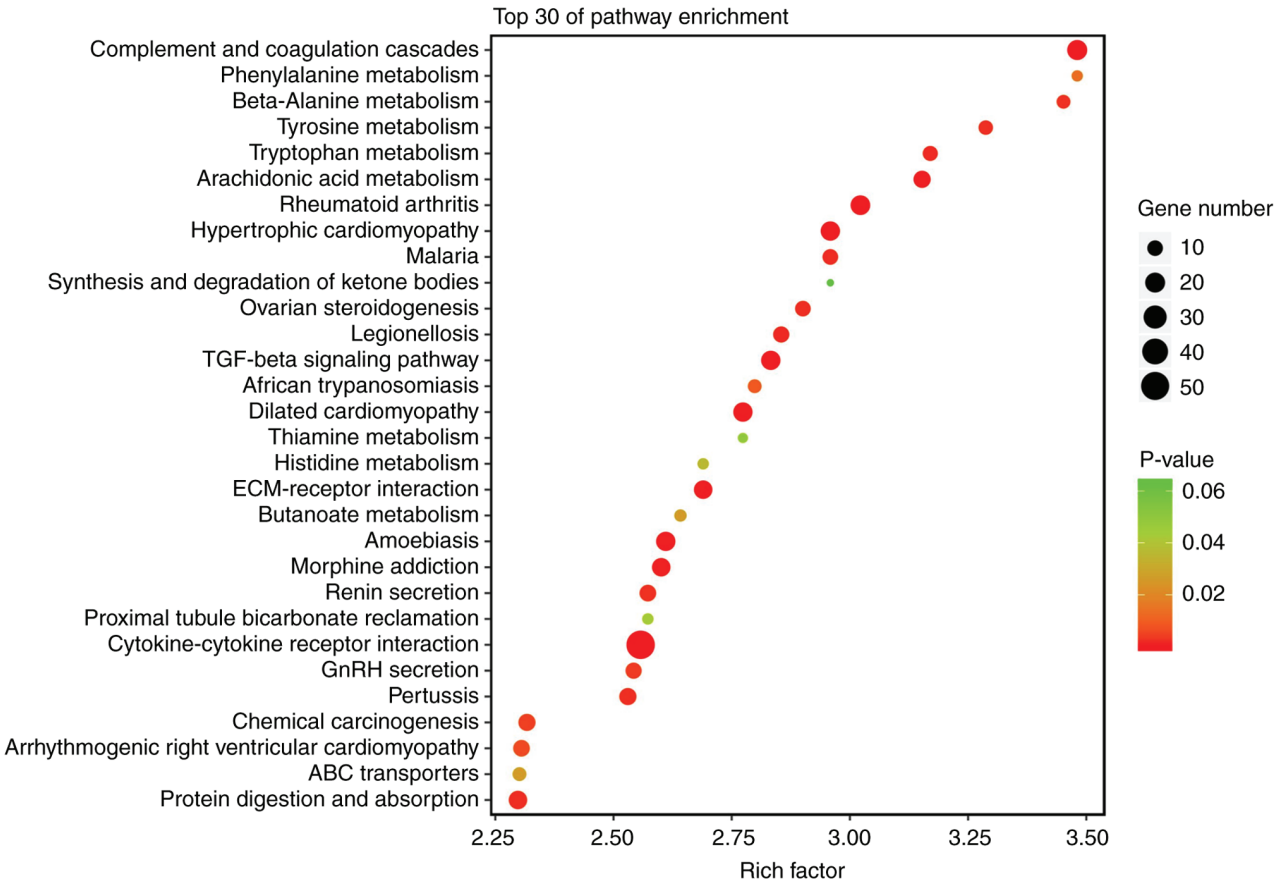

Figure 5. Top 30 KEGG pathways of dysregulated genes. The top 30 GO terms were screened using the rich factor. The size of circles indicates the gene number and the color indicates the P-value. KEGG, Kyoto Encyclopedia of Genes and Genomes.

Table III. Bioinformatical analysis of genes enriched in cell motility-related biological processes.

GO/ pathway_ID	GO_term/ pathway_DES	diff_gene_ in_this_pathway	Up_ genes	Down_ genes	gene_UP_list	gene_DOWN_list	rich_ factor	P-value
GO:2000145	Regulation of cell motility	110	50	60	SEMA6B, GREM1, SERPINB3, SERPINE2, CXCL12[a], TNFAIP6, ITGA2[a], PAX6, JUN, DRD2, PTGS2, ACVRL1, BDKRB1[a], LBP, DNAI3, CGA, CDH5, BMP5, VEGFA, PGF, PLXNA4, CXCL8, TNFRSF18, NRG1, CXCL10, POSTN, CLDN3, WAS, STC1, LAMA2, CORO1A, LGR6, CD200, HGF, DUSP3, SRCIN1, IL24, SEMA3G, SMIM22, IL1R1, NTRK3, CCL8, BMP2, CYGB, ATP1B2, MEOX2, SPOCK2, IL1B, GPR183, EREG	S100A14, PTPRR, ANGPTL3, EDN1, FGF22[a], TACSTD2, F3, DUSP22, NEDD9, PTGER4, HMOX1, DOCK8, MIR503, SMURF2, IL34, GPNMB, SERPINE1, TF, ACKR3, IL12A, ADTRP, FLT4, MMP28, IGFBP3, SYNPO2, MIR221, RARRES2, AQP1, MIR29A, PDGFD[a], SEMA3E, DCN, MGAT3, TAC4, FGF5[a], ONECUT1, FLT1, FGF17[a], IL23A, MIR27B, STK26, ANGPT1, PODN, NOG, FAM110C, CCN1, SEMA6A, FGF18[a], SULF1, FGF1[a], TPM1, PPARGC1A, ADRA2A, PLXNC1, GAS6, DRD1, BST1, RHOJ, MSTN, CASS4	1.394	0.001
hsa04810	Regulation of actin cytoskeleton	22	7	15	CXCL12[a], ITGA2[a], ITGB7, ITGB2, FGFR4, ARHGEF4, BDKRB1[a]	CHRM4, SCIN, ITGB8, MYH11, MYL9, FGF5[a], FGF22[a], ITGA1, FGF17[a], ACTR3C, ITGA11, PDGFD[a], VAV3, FGF1[a], FGF18[a]	1.493	0.059

[a]Nine genes overlapped in the two processes.

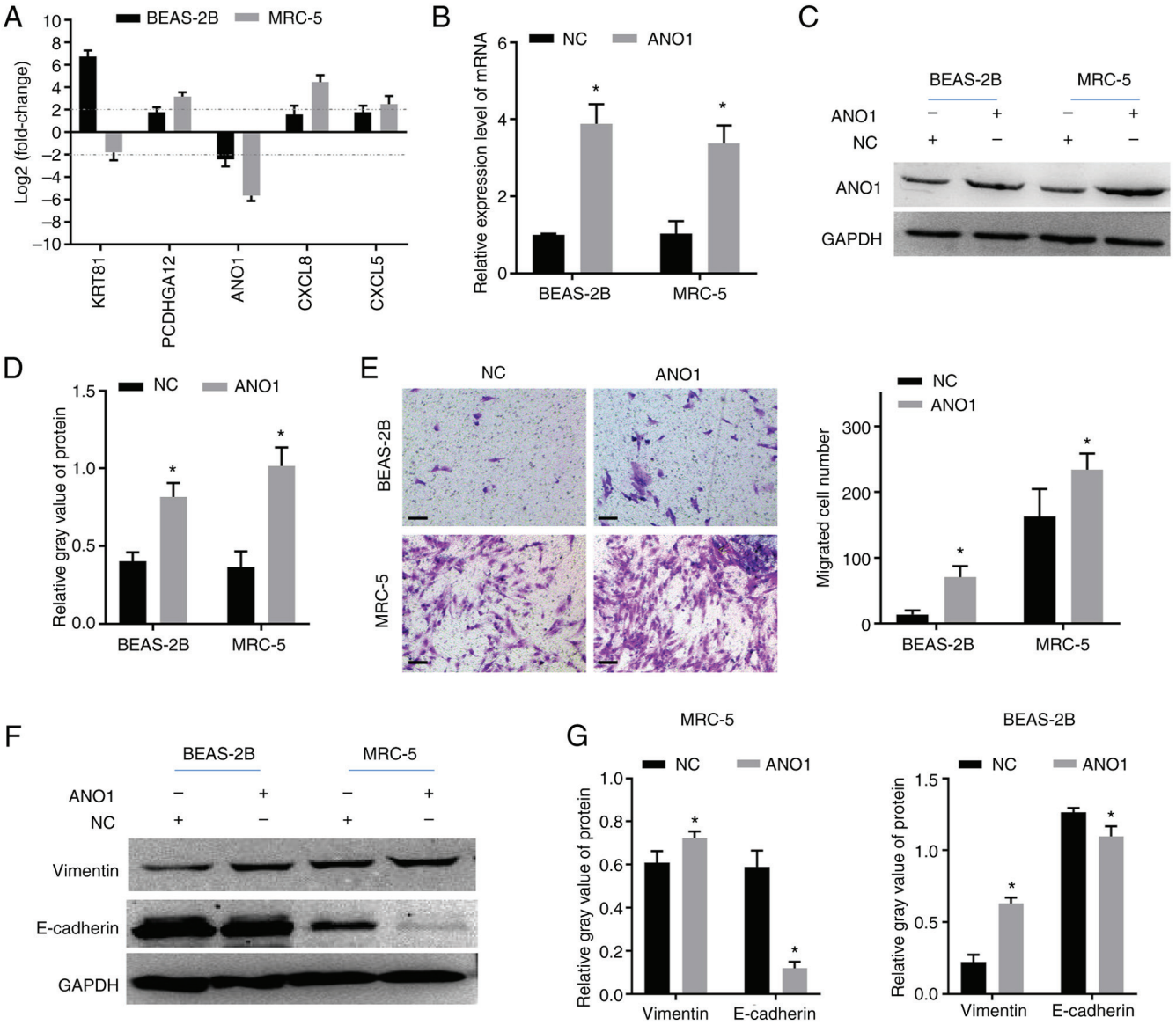

Figure 6. Overexpression of ANO1 promotes the EMT of lung cells. (A) qPCR validation of top five known genes in two lung cells (n=3). The fold-change indicates the cells treated with TGF-β1 + exosome vs. cells treated with TGF-β1. Cells were transfected with an overexpression vector of ANO1 (pcDNA3.1-ANO1) or blank vector (NC), respectively. (B) qPCR was used to confirm the overexpression effect of ANO1 in the two types of cells (n=3). (C) Western blot analysis was used to detect the protein level of ANO1 (n=3). (D) Quantification analysis result of ANO1 protein level. (E) Transwell assay was performed to evaluate the migration ability (n=3). Scale bar, 100 μm. (F) Western blot analysis was used to detect the protein level of the EMT markers (n=3). (G) Quantification analysis result of protein level of the EMT markers. *P<0.05. ANO1, anoctamin-1; EMT, epithelial-mesenchymal transition; qPCR, quantitative PCR; NC, negative control.

Another two migration-related GO terms and KEGG pathways were also extracted, since little evidence could be found associated with EMT in the top 30 terms and 30 pathways. As shown in Table III, 110 of the genes were enriched in the regulation of cell motility and 22 genes were involved in the pathway responsible for the regulation of the actin cytoskeleton. Next, nine overlapped genes (in red, Table III) were obtained through comparing the genes in the two collections, including three upregulated genes (CXCL12, ITGA2 and BDKRB1) and six downregulated ones (FGF5, FGF22, FGF17, PDGFD, FGF1 and FGF18). These may might be involved in the EMT process reversed by exosomes.

Overexpression of ANO1 promotes the EMT of lung cells. Since the top 20 dysregulated genes had much higher FC (abs) values, the first five known genes, excluding the unknown gene AP005263.1, were selected for qPCR validation. As a result, the log2FC values of four genes were consistent in the two lung cells. The FC (abs) values of ANO1 in the two cells were both higher than 4, whereas the value of the other three genes in BEAS-2B or MRC-5 was always lower than 4 (Fig. 6A). Therefore, ANO1 was selected for further analysis. The qPCR and western blotting results showed that ANO1 was successfully overexpressed in the two types of cells. As shown in Fig. 6B-D, the mRNA expression level was enhanced by 2-3 fold and the ANO1 protein level was also significantly increased. Further assays indicated that the migration abilities were both significantly enhanced after the overexpression of ANO1, along with increased levels of vimentin and downregulated levels of E-cadherin (Fig. 6E-G). These results suggest

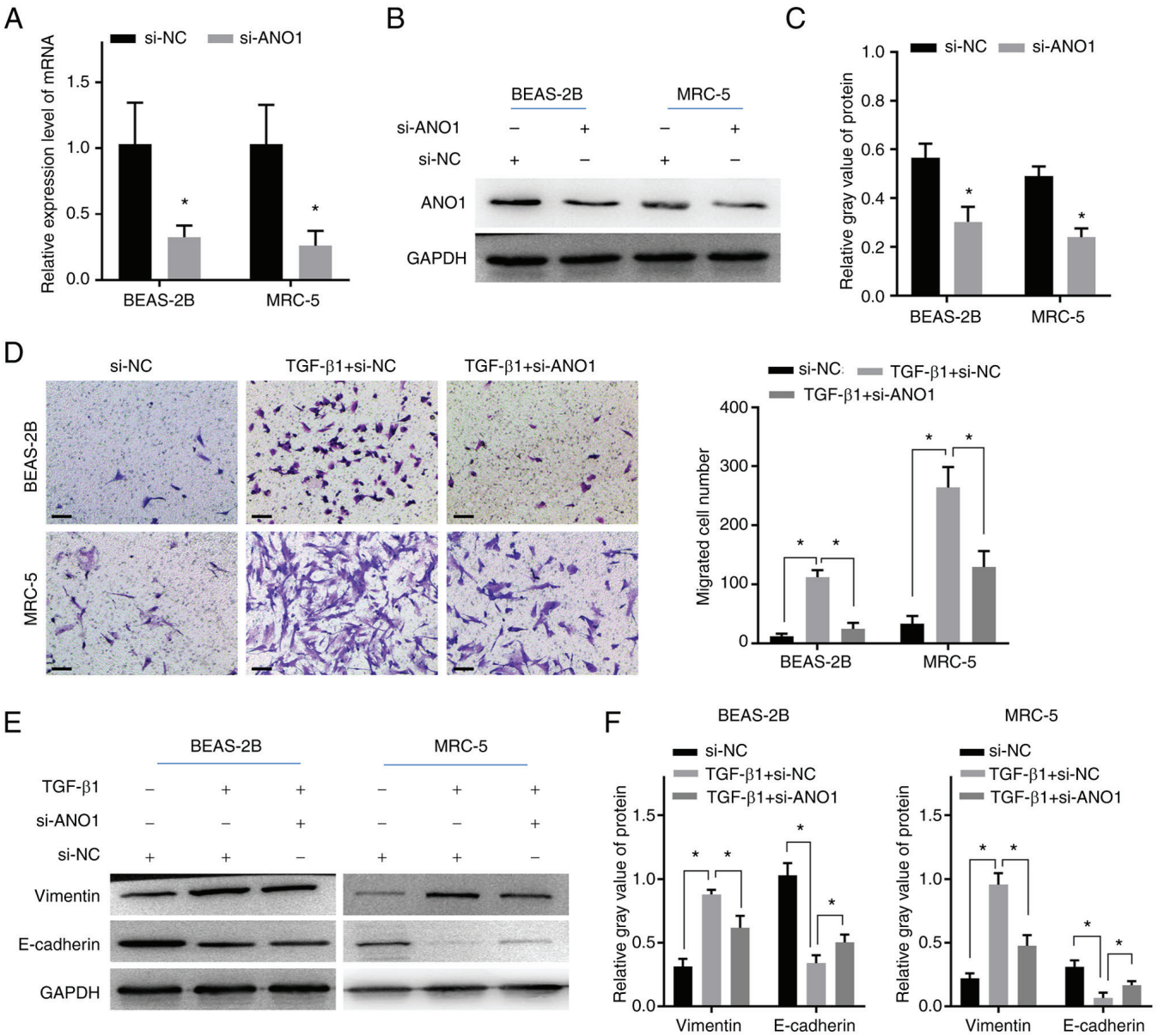

Figure 7. Knockdown of ANO1 inhibited the TGF-β1-induced EMT of lung cells. (A) qPCR was used to confirm the interference effect of ANO1 in the two types of cells (n=3). (B) Western blot analysis was used to detect the protein level of ANO1 in the two types of cells (n=3). (C) Quantification analysis result of ANO1 protein level. (D) Transwell assay was performed to evaluate the role of silencing ANO1 on migration ability (n=3). Scale bar, 100 μm. (E) Western blot analysis was used to detect the role of silencing ANO1 on the protein level of the EMT markers (n=3). (F) Quantification analysis result of protein level of the EMT markers. *P<0.05. ANO1, anoctamin-1; EMT, epithelial-mesenchymal transition; qPCR, quantitative PCR; si, short interfering; NC, negative control.

that the overexpression of ANO1 could induce the EMT and enhance the migration ability of lung cells.

Knockdown of ANO1 inhibits the TGF-β1-induced EMT of lung cells. To further confirm the role of ANO1, its expression was evaluated in lung cells. The qPCR results indicated that the expression level of ANO1 was reduced by ~60% (Fig. 7A). Consistently, its protein level was also significantly decreased (Fig. 7B and C). Next, ANO1 knockdown cells were further treated with TGF-β1 for 24 h. The Transwell results indicated that the migration ability of BEAS-2B in the si-NC + TGF-β1 group showed a significant enhancement compared with si-NC group, whereas the knockdown of ANO1 caused a weakness of migration ability compared with those in the si-NC + TGF-β1 group (Fig. 7D). The migration ability of MRC-5 also showed a similar trend (Fig. 7D). In addition, the knockdown of ANO1 in two lung cells also inhibited the EMT induced by TGF-β1 (Fig. 7E and F). These results suggest that the downregulation of ANO1 induced by exosomes is an important mechanism for the suppression of the TGF-β1-induced EMT by exosomes.

Airway basal cell-derived exosomes treatment ameliorates pulmonary fibrosis and inhibits the upregulation of ANO1 induced by bleomycin. H&E and Masson's trichrome staining results indicated that, bleomycin treatment resulted in interstitial thickening, infiltration of inflammatory cells and collagen deposition (indicated by arrows; Fig. 8A and B). Typical fibrosis progression markers COL1A1 and FN1 were both significantly enhanced in model group, compared with control group (Fig. 8C and D).

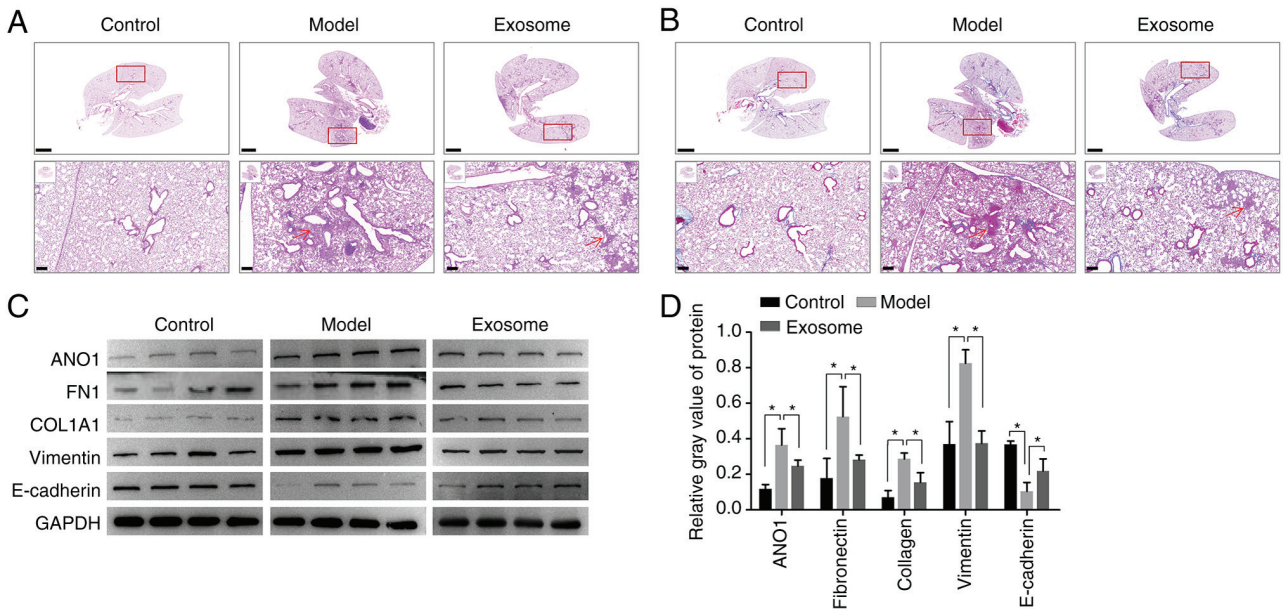

Figure 8. Airway basal cell-derived exosome treatment ameliorated pulmonary fibrosis and inhibited the upregulation of ANO1 induced by bleomycin. Mice were treated with bleomycin (2 U/kg) or further treated with airway basal cell-derived exosomes ($10x10^9$ particles/kg) for 7 days and lung tissues were collected at 21 days post bleomycin treatment and used for the following assays. (A) Hematoxylin and eosin staining of lung tissues. Upper scale bar, 2,000 μm; lower scale bar, 200 μm. (B) Masson's trichrome staining of lung tissues. Upper scale bar, 2,000 μm; lower scale bar, 200 μm. (C) Western blot analysis of protein levels of fibrosis and EMT markers as well as ANO1 (n=4). (D) Quantification analysis result of protein levels. *P<0.05. ANO1, anoctamin-1; EMT, epithelial-mesenchymal transition.

In addition, a significant increase of vimentin expression level as well as the reduction of E-cadherin was also found following bleomycin treatment (Fig. 8C and D), which indicated the EMT of lung cells and the progression of fibrosis. Notably, bleomycin treatment also caused a significant upregulation of ANO1 (Fig. 8C and D).

Following exosome treatment for 7 consecutive days, the fibrosis level was reduced, with fewer interstitial thickening and collagen deposition were observed in exosome group (indicated by arrows; Fig. 8A and B). Consistently, the protein levels of fibrosis makers were both decreased and the EMT level was also alleviated (Fig. 8C and D). Furthermore, exosome treatment also reduced the expression level of ANO1. These results indicated that airway basal cell-derived exosomes could ameliorate pulmonary fibrosis and inhibited the upregulation of ANO1, basically consistent with the *in vitro* results.

Discussion

In recent years, exosomes derived from MSCs and other cells have increasingly received attention compared with the cells themselves due to the number of advantages of exosomes in clinical applications. First, these extracellular products can avoid the risks associated with whole-cell transplantation, as well as being non-oncogenic and less immunogenic compared with living cells (24). Second, the procedures used for the sterilization, handling and storage of exosomes are simpler, thereby reducing manufacturing costs (25). The present study focused on exosomes derived from the airway basal cells and found that they could inhibit the TGF-β1-induced EMT of lung epithelial cells and fibroblasts and bleomycin-induced pulmonary fibrosis, providing a potential therapeutic option for patients with IPF.

The pathological process of IPF is very complex and involves the participation of various inflammation factors and cytokines, among which TGF-β1 plays a predominant role. The exposure of lung cells to TGF-β1 generally results in the activation of cells and EMT and ECM accumulation, which is a widely used as an *in vitro* model. The occurrence of EMT in damaged epithelial cells not only causes continuous mesenchymal cell activation and matrix remodeling, but also alterations of tissue function once they separate from neighboring cells and migrate to adjacent tissues (26). In fibroblasts, EMT is regarded as an important mechanism leading to the generation of myofibroblasts (27). Therefore, the present study focused on reversing the EMT of lung cells, in contrast to previous studies. As a result, it was found that the exposure of lung cells caused the occurrence of EMT, while further treatment with exosomes inhibited the EMT process.

Metabolic reprogramming is regarded as a hallmark of cancer that contributes to tumorigenesis and disease progression. It has been reported that metabolic reprogramming occurs during TGFβ-induced EMT in IPF and non-small cell lung carcinoma (NSCLC) (28,29). For instance, TGFβ treatment results in an increased activity of glycolytic enzymes, thus enhancing glycolysis metabolism, as well as the TCA cycle. Notably, extensive metabolic changes have also been observed after exosome treatment (29). The results of the bioinformatical analysis indicated that the dysregulated genes were predominantly enriched in the metabolism of amino acids, including glycine catabolic process, as well as tryptophan metabolism. Glycine and tryptophan are classic TCA cycle metabolites associated with EMT-driven NSCLC progression and prognosis (30). Therefore, exosomes may inhibit the metabolic reprogramming induced by TGF-β1 by regulating

the expression level of genes involved in the metabolism of certain key amino acids.

Among the nine overlapped genes enriched in cell motility-related terms and pathways, five belonged to fibroblast growth factors (FGFs). FGFs are critical in controlling cell proliferation, migration and differentiation through the activation of surface receptors (31). It has been reported that FGF1 is elevated in patients with IPF (32) and FGF18 is able to promote the migration of lung fibroblasts (33). Therefore, the downregulation of FGF1 and FGF18 may also be involved in the inhibition of EMT following exosome treatment. Furthermore, 18 genes were found to be enriched in the TGF-β signaling pathway and the dysregulation of these genes also played important roles in the signaling transduction of TGF-β1. Compared with the nine overlapped genes enriched in motility-related biological processes, the top 20 dysregulated genes had a much higher fold-change, as well as a more significant P-value. Therefore, focusing on the top 20 ones would obtain a consistent validation result of the two types of cells. As a result, four genes among the five tested showed a consistent fold-change in the two cells treated with exosomes, indicating the RNA sequencing result was reliable.

ANO1, also known as transmembrane protein 16A, is recognized as a Ca^{2+}-activated chloride channel and is widely expressed in epithelial cells and smooth muscle cells (18). In the field of fibrosis, research on ANO1 is centered on cystic fibrosis due to its fundamental role in regulating mucus secretion and he production of epithelial and ciliated cells (34,35). The role of ANO1 in the function of lung fibroblasts has also been reported. For instance, the exposure of human lung fibroblasts to TGF-β results in a sharp increase in the mRNA levels of ANO1 and the inhibition of ANO1 via the inhibitor tannic acid causes the downregulation of smooth muscle actin and fibronectin, markers of myofibroblast differentiation (36). Additionally, the alteration of ANO1 is also able to regulate the proliferation and apoptosis of lung fibroblasts in a mouse model of IPF (37). These studies highlight the vital role of ANO1 in lung fibrosis. However, whether ANO1 regulates the EMT or migration ability of lung cells is less investigated. The present study found that the overexpression of ANO1 induced the EMT of lung epithelial cells and fibroblasts, while the silencing of ANO1 reversed the EMT induced by TGF-β1. Consistent with the present study, the overexpression of ANO1 has been previously reported to cause the EMT and stronger migration ability of various cancer cells, including lung cancer cells (38,39).

Bleomycin-induced pulmonary fibrosis is a widely used model, which closely mimics the pathological features of human IPF. 9-days treatment of bleomycin initiates the fibrotic response, resulting in the expression of pro-fibrotic factors (40), followed by the deposition of collagen (41). The *in vivo* assay of the present study indicated that exosome treatment effectively inhibited bleomycin-induced pulmonary fibrosis, consistent with *in vitro* results. It was also found that bleomycin treatment resulted in the upregulation of ANO1 and further exosome treatment ameliorated its upregulation. Notably, the protein level of TGF-β1 is found to be significantly enhanced in bleomycin-induced pulmonary fibrosis models (42,43). The *in vitro* assay of the present study confirmed that knockdown of ANO1 inhibited the TGF-β1-induced EMT of lung cells. Therefore, the upregulation of ANO1 in pulmonary fibrosis model may be related to the increased level of TGF-β1.

The reduction of ANO1 protein level in exosome group indicated that exosome could inhibit the expression of ANO1, but it is difficult to explain if this reduction is directly or indirectly caused by the exosomes. It is reported that microRNAs (miR), miR-142-3p (44) and miR-769-5p (45), carried by exosomes could directly bind with the 3'-UTR of TGF-β1 mRNA, thereby downregulating its mRNA level. In addition, the expression level of ANO1 could also be inhibited by miR-9 (37) and miR-381 (46). Therefore, the downregulation of ANO1 in the mice model may be the synthesis results of the molecules/miRNAs carried by exosomes and miRNAs targeting ANO1 may be just one of the mechanisms, which also required further investigations.

The present study has some limitations. The screening of dysregulated genes was based on one replicate of the two different cell samples. Herein, the addition of one replicate for sequencing would improve the reliability of the screened genes. Another limitation is that only the |log2FC| value of gene was taken as the major factor for candidate gene selection, while the functional annotation analysis was neglected. A combination of the FC value and functional annotation analysis for gene selection should be included in future studies. In addition, the effective exosome contents were not detected, which also deserved further investigation. The last limitation is that, only EMT markers were detected, while other cytokines related to EMT were not detected.

In the present study, airway basal cell-derived exosomes were found to suppress the TGF-β1-induced EMT of lung cells and bleomycin-induced pulmonary fibrosis by downregulating ANO1. Thus, these exosomes represent a potential therapeutic option for patients with IPF. Furthermore, the gene expression profile of exosome-treated cells was elucidated and the corresponding dysregulated genes provide insights into the mechanisms of exosomes.

Acknowledgements

Not applicable.

Funding

No funding was received.

Availability of data and materials

The data generated in the present study may be requested from the corresponding author. The raw data of RNA sequencing was deposited in the SRA database and is accessible at https://www.ncbi.nlm.nih.gov/sra/PRJNA1051029.

Authors' contributions

TR and SW designed the study. XG, ZL and SS performed the experiments. XG and ZL collected the data. XG and SS analyzed the data. XG and SW confirm the authenticity of all

the raw data. All authors contributed to the preparation of the manuscript, and read and approved the final manuscript.

Ethics approval and consent to participate

All experimental procedures were approved by the Animal Welfare Ethics Committee of Shanghai Sixth People's Hospital (approval no. 2023-0374).

Patient consent for publication

Not applicable.

Competing interests

The authors declare that they have no competing interests.

References

1. Abuserewa ST, Duff R and Becker G: Treatment of idiopathic pulmonary fibrosis. Cureus 13: e15360, 2021.
2. Glass DS, Grossfeld D, Renna HA, Agarwala P, Spiegler P, DeLeon J and Reiss AB: Idiopathic pulmonary fibrosis: Current and future treatment. Clin Respir J 16: 84-96, 2022.
3. Mattoo H and Pillai S: Idiopathic pulmonary fibrosis and systemic sclerosis: Pathogenic mechanisms and therapeutic interventions. Cell Mol Life Sci 78: 5527-5542, 2021.
4. Spagnolo P, Kropski JA, Jones MG, Lee JS, Rossi G, Karampitsakos T, Maher TM, Tzouvelekis A and Ryerson CJ: Idiopathic pulmonary fibrosis: Disease mechanisms and drug development. Pharmacol Ther 222: 107798, 2021.
5. Purghè B, Manfredi M, Ragnoli B, Baldanzi G and Malerba M: Exosomes in chronic respiratory diseases. Biomed Pharmacother 144: 112270, 2021.
6. Kadota T, Yoshioka Y, Fujita Y, Araya J, Minagawa S, Hara H, Miyamoto A, Suzuki S, Fujimori S, Kohno T, *et al*: Extracellular vesicles from fibroblasts induce epithelial-cell senescence in pulmonary fibrosis. Am J Respir Cell Mol Biol 63: 623-636, 2020.
7. Zhu L, Chen Y, Chen M and Wang W: Mechanism of miR-204-5p in exosomes derived from bronchoalveolar lavage fluid on the progression of pulmonary fibrosis via AP1S2. Ann Transl Med 9: 1068, 2021.
8. Kadota T, Fujita Y, Araya J, Watanabe N, Fujimoto S, Kawamoto H, Minagawa S, Hara H, Ohtsuka T, Yamamoto Y, *et al*: Human bronchial epithelial cell-derived extracellular vesicle therapy for pulmonary fibrosis via inhibition of TGF-β-WNT crosstalk. J Extracell Vesicles 10: e12124, 2021.
9. Samarelli AV, Tonelli R, Heijink I, Martin Medina A, Marchioni A, Bruzzi G, Castaniere I, Andrisani D, Gozzi F, Manicardi L, *et al*: Dissecting the Role of mesenchymal stem cells in idiopathic pulmonary fibrosis: Cause or solution. Front Pharmacol 12: 692551, 2021.
10. Hoang DM, Pham PT, Bach TQ, Ngo ATL, Nguyen QT, Phan TTK, Nguyen GH, Le PTT, Hoang VT, Forsyth NR, *et al*: Stem cell-based therapy for human diseases. Signal Transduct Target Ther 7: 272, 2022.
11. Ha DH, Kim HK, Lee J, Kwon HH, Park GH, Yang SH, Jung JY, Choi H, Lee JH, Sung S, *et al*: Mesenchymal stem/stromal cell-derived exosomes for immunomodulatory therapeutics and skin regeneration. Cells 9: 1157, 2020.
12. Zhang E, Geng X, Shan S, Li P, Li S, Li W, Yu M, Peng C, Wang S, Shao H and Du Z: Exosomes derived from bone marrow mesenchymal stem cells reverse epithelial-mesenchymal transition potentially via attenuating Wnt/β-catenin signaling to alleviate silica-induced pulmonary fibrosis. Toxicol Mech Methods 31: 655-666, 2021.
13. Harrell CR, Miloradovic D, Sadikot R, Fellabaum C, Markovic BS, Miloradovic D, Acovic A, Djonov V, Arsenijevic N and Volarevic V: Molecular and cellular mechanisms responsible for beneficial effects of mesenchymal stem cell-derived product 'Exo-d-MAPPS' in attenuation of chronic airway inflammation. Anal Cell Pathol (Amst) 2020: 3153891, 2020.
14. Sengupta V, Sengupta S, Lazo A, Woods P, Nolan A and Bremer N: Exosomes derived from bone marrow mesenchymal stem cells as treatment for severe COVID-19. Stem Cells Dev 29: 747-754, 2020.
15. Ma Q, Ma Y, Dai X, Ren T, Fu Y, Liu W, Han Y, Wu Y, Cheng Y, Zhang T and Zuo W: Regeneration of functional alveoli by adult human SOX9$^+$ airway basal cell transplantation. Protein Cell 9: 267-282, 2018.
16. Lee C, Mitsialis SA, Aslam M, Vitali SH, Vergadi E, Konstantinou G, Sdrimas K, Fernandez-Gonzalez A and Kourembanas S: Exosomes mediate the cytoprotective action of mesenchymal stromal cells on hypoxia-induced pulmonary hypertension. Circulation 126: 2601-2611, 2012.
17. Kropski JA and Blackwell TS: Progress in understanding and treating idiopathic pulmonary fibrosis. Annu Rev Med 70: 211-224, 2019.
18. Takayama Y, Derouiche S, Maruyama K and Tominaga M: Emerging perspectives on pain management by modulation of TRP channels and ANO1. Int J Mol Sci 20: 3411, 2019.
19. Zuo W, Zhang T, Wu DZ, Guan SP, Liew AA, Yamamoto Y, Wang X, Lim SJ, Vincent M, Lessard M, *et al*: p63(+)Krt5(+) distal airway stem cells are essential for lung regeneration. Nature 517: 616-620, 2015.
20. R Core Team. R: A language and environment for statistical computing. R Foundation for Statistical Computing, Vienna, Austria, 2019.
21. Javellana M, Eckert MA, Heide J, Zawieracz K, Weigert M, Ashley S, Stock E, Chapel D, Huang L, Yamada SD, *et al*: Neoadjuvant chemotherapy induces genomic and transcriptomic changes in ovarian cancer. Cancer Res 82: 169-176, 2022.
22. Livak KJ and Schmittgen TD: Analysis of relative gene expression data using real-time quantitative PCR and the 2(-Delta Delta C(T)) method. Methods 25: 402-408, 2001.
23. Liu P, Miao K, Zhang L, Mou Y, Xu Y, Xiong W, Yu J and Wang Y: Curdione ameliorates bleomycin-induced pulmonary fibrosis by repressing TGF-beta-induced fibroblast to myofibroblast differentiation. Respir Res 21: 58, 2020.
24. Giebel B, Kordelas L and Börger V: Clinical potential of mesenchymal stem/stromal cell-derived extracellular vesicles. Stem Cell Investig 4: 84, 2017.
25. Gimona M, Pachler K, Laner-Plamberger S, Schallmoser K and Rohde E: Manufacturing of human extracellular vesicle-based therapeutics for clinical use. Int J Mol Sci 18: 1190, 2017.
26. Xie L and Zeng Y: Therapeutic potential of exosomes in pulmonary fibrosis. Front Pharmacol 11: 590972, 2020.
27. Hu L, Ding M and He W: Emerging therapeutic strategies for attenuating tubular EMT and kidney fibrosis by targeting Wnt/β-catenin signaling. Front Pharmacol 12: 830340, 2022.
28. Zhao H, Dennery PA and Yao H: Metabolic reprogramming in the pathogenesis of chronic lung diseases, including BPD, COPD, and pulmonary fibrosis. Am J Physiol Lung Cell Mol Physiol 314: L544-L554, 2018.
29. Hua W, Ten Dijke P, Kostidis S, Giera M and Hornsveld M: TGFβ-induced metabolic reprogramming during epithelial-to-mesenchymal transition in cancer. Cell Mol Life Sci 77: 2103-2123, 2020.
30. Giannos P, Kechagias KS and Gal A: Identification of prognostic gene biomarkers in non-small cell lung cancer progression by integrated bioinformatics analysis. Biology (Basel) 10: 1200, 2021.
31. Seitz T and Hellerbrand C: Role of fibroblast growth factor signalling in hepatic fibrosis. Liver Int 41: 1201-1215, 2021.
32. MacKenzie B, Korfei M, Henneke I, Sibinska Z, Tian X, Hezel S, Dilai S, Wasnick R, Schneider B, Wilhelm J, *et al*: Increased FGF1-FGFRc expression in idiopathic pulmonary fibrosis. Respir Res 16: 83, 2015.
33. Joannes A, Brayer S, Besnard V, Marchal-Somme J, Jaillet M, Mordant P, Mal H, Borie R, Crestani B and Mailleux AA: FGF9 and FGF18 in idiopathic pulmonary fibrosis promote survival and migration and inhibit myofibroblast differentiation of human lung fibroblasts in vitro. Am J Physiol Lung Cell Mol Physiol 310: L615-L629, 2016.
34. Kunzelmann K, Ousingsawat J, Cabrita I, Doušová T, Bähr A, Janda M, Schreiber R and Benedetto R: TMEM16A in cystic fibrosis: Activating or inhibiting? Front Pharmacol 10: 3, 2019.
35. Danahay H and Gosling M: TMEM16A: An alternative approach to restoring airway anion secretion in cystic fibrosis? Int J Mol Sci 21: 2386, 2020.

36. Dulin NO, Smolyaninova LV and Orlov SN: Control of lung myofibroblast transformation by monovalent ion transporters. Curr Top Membr 83: 15-43, 2019.
37. Dai WJ, Qiu J, Sun J, Ma CL, Huang N, Jiang Y, Zeng J, Ren BC, Li WC and Li YH: Downregulation of microRNA-9 reduces inflammatory response and fibroblast proliferation in mice with idiopathic pulmonary fibrosis through the ANO1-mediated TGF-β-Smad3 pathway. J Cell Physiol 234: 2552-2565, 2019.
38. Chen W, Gu M, Gao C, Chen B, Yang J, Xie X, Wang X, Sun J and Wang J: The prognostic value and mechanisms of TMEM16A in human cancer. Front Mol Biosci 8: 542156, 2021.
39. Guo S, Chen Y, Shi S, Wang X, Zhang H, Zhan Y and An H: Arctigenin, a novel TMEM16A inhibitor for lung adenocarcinoma therapy. Pharmacol Res 155: 104721, 2020.
40. Chaudhary NI, Schnapp A and Park JE: Pharmacologic differentiation of inflammation and fibrosis in the rat bleomycin model. Am J Respir Crit Care Med 173: 769-776, 2006.
41. Vats A and Chaturvedi P: The regenerative power of stem cells: Treating bleomycin-induced lung fibrosis. Stem Cells Cloning 16: 43-59, 2023.
42. Qian W, Cai X, Qian Q, Zhang W and Wang D: Astragaloside IV modulates TGF-β1-dependent epithelial-mesenchymal transition in bleomycin-induced pulmonary fibrosis. J Cell Mol Med 22: 4354-4365, 2018.
43. Cutroneo KR, White SL, Phan SH and Ehrlich HP: Therapies for bleomycin induced lung fibrosis through regulation of TGF-beta1 induced collagen gene expression. J Cell Physiol 211: 585-589, 2007.
44. Huang C, Zhao L, Xiao Y, Tang Z, Jing L, Guo K, Tian L and Zong C: M2 macrophage-derived exosomes carry miR-142-3p to restore the differentiation balance of irradiated BMMSCs by targeting TGF-β1. Mol Cell Biochem: Jun 3, 2023 (Epub ahead of print).
45. Ni N, Ma W, Tao Y, Liu J, Hua H, Cheng J, Wang J, Zhou B and Luo D: Exosomal MiR-769-5p exacerbates ultraviolet-induced bystander effect by targeting TGFBR1. Front Physiol 11: 603081, 2020.
46. Cao Q, Liu F, Ji K, Liu N, He Y, Zhang W and Wang L: MicroRNA-381 inhibits the metastasis of gastric cancer by targeting TMEM16A expression. J Exp Clin Cancer Res 36: 29, 2017.